Conservative phase-field lattice Boltzmann model for interface tracking equation

Martin Geier, Abbas Fakhari, and Taehun Lee

Phys. Rev. E **91**, 063309 — Published 17 June 2015

DOI: 10.1103/PhysRevE.91.063309

A conservative phase-field lattice Boltzmann model for interface tracking equation

Martin Geier

*TU Braunschweig, Institute for Computational Modeling in Civil Engineering (iRMB), TU-Braunschweig, Pockelsstr. 3, 38106 Braunschweig, Germany**

Abbas Fakhari and Taehun Lee

Department of Mechanical Engineering, the City College of the City University of New York, New York, NY 10031, USA†

Abstract

Based on the phase-field theory, we propose a conservative lattice Boltzmann method to track the interface between two different fluids. The presented model recovers the conservative phase-field equation and conserves mass locally and globally. Two entirely different approaches are used to calculate the gradient of the phase field, which is needed in computation of the normal to the interface. One approach uses finite-difference stencils similar to many existing lattice Boltzmann models for tracking the two-phase interface, while the other one invokes central moments to calculate the gradient of the phase field without any finite differences involved. The former approach suffers from the non-locality of the collision operator while the latter is entirely local making it highly suitable for massive parallel implementation. Several benchmark problems are carried out to assess the accuracy and stability of the proposed model.

PACS numbers: 47.11.Qr, 47.11.-j

Keywords: interface tracking; diffuse-interface theory; phase-field modeling; conservative phase-field equation; conservative lattice Boltzmann method

* geier@irmb.tu-bs.de

† thlee@ccny.cuny.edu; https://sites.google.com/site/leeccny/home

I. INTRODUCTION

Phase-field models are used to identify and track multiple domains with different physical properties for a given velocity field. The main application of phase-field models is in simulation of multiphase (liquid/liquid or liquid/gas) flows. The phase-field equation is then an add-on to the Navier-Stokes (or other governing) equations. In addition to identification of each phase, the phase-field variable is often used to identify certain properties of the interface between different fluids such as gradients and curvature, which might be required to model surface tension or other interfacial properties. Both Navier-Stokes and phase-field equations can be solved using many different numerical schemes. In this paper we use the lattice Boltzmann method (LBM) [1] to solve the phase-field equation for a given velocity field.

The LBM is a numerical scheme for solving general transient transport problems. The LBM employs a local discrete distribution function in momentum space that undergoes a two-step evolution of repeated propagation and collision. In the propagation or streaming step the distributions move according to their respective momenta to the neighboring nodes on the Cartesian grid. Due to the exact correspondence between the discretization of the momentum space and the Cartesian grid this propagation is numerically exact and conservative. In the collision step the distributions belonging to a lattice node are locally rearranged. From the numerical point of view, one interesting property of the LBM is that all non-locality (propagation) is linear and all non-linearity (collision) is local. Unfortunately, this appealing feature is lost in many attempts to apply the LBM to multiphase flows. The reason for this is that most phase-field models depend on the computation of the gradient of the phase indicator. This computation is often done by finite-difference (FD) schemes such that the majority of multiphase lattice Boltzmann (LB) models are hybrid FD-LBM [2–6].

Spencer *et al.* [7] computed the first moment of the density of a multi-component LB scheme to approximate the normal of the phase interface. This approach does not take into account the fact that the fluid velocity is also encoded in the first moment. It is based on the assumption that the gradient of the component density at the interface is much larger than the influence of the velocity, so that the fluid velocity can be neglected altogether. Tölke *et al.* [8] used a phase-field lattice Boltzmann equation (LBE) and computed the gradient of the interface from the non-equilibrium part of the first moment of the phase distribution.

This approach computes the interface normal independently from the fluid velocity and is hence expected to be more accurate than the method proposed in Ref. [7] with respect to Galilean invariance. However, Tölke *et al.* [8] implemented their model for creeping flow only and the Galilean invariance was not investigated.

Every equation that can be solved by LBM can also be solved by classical finite-difference method (FDM). In general, the computational effort and the numerical accuracy of these two different approaches are expected to be similar but might depend on the respective details of their implementation. A good implementation of one will always prevail a poor implementation of the other. In general, FDM is expected to need less memory than LBM because the former requires fewer primary variables per computational node, while the latter uses a distribution function of which the primary variables (phase-field, density, and momentum) are statistical moments. On the other hand, implementation of conservation laws in an exactly conservative fashion is trivial in LBM. This is particularly useful when closed domains without Dirichlet boundary conditions are considered. While both LBM and FDM have their own advantages, it is not favorable to use a combination of them because a hybrid scheme usually inherits the respective downsides of both methods. Unfortunately, this is frequently done in the existing LB models for multiphase flows.

From the diffuse-interface modeling point of view, interface tracking equations usually rely on the Cahn-Hilliard theory [9] because it implies conservation of the phase indicator and therefore conservation of mass. The Cahn-Hilliard equation, however, is not suitable for local computations in LB framework because it includes fourth-order spacial derivatives, which, according to the asymptotic analysis, cannot be determined from central moments. On the other hand, the Allen-Cahn equation [10] only requires second-order derivatives which are locally accessible in LB framework. Although the Allen-Cahn equation is not originally conservative, recently it has been modified to a phase-field model [11] and reshaped into a conservative form [12]. Therefore, it is possible to formulate the conservative phase-field equation in the context of LBM by defining the phase indicator as a collision invariant.

In this paper, we propose phase-field-based LB models with and without local computation of the interface normal. We compare the calculation of the phase-field gradients by using moments and by using supplementary finite differences. The version of the model that uses central moments to compute the interface normal is a native LBM with the desired features: all non-locality is linear, all non-linearity is local, and the read-once-write-once

time stepping property is maintained. In the version that uses FD to compute the interface normal we use isotropic central-differences [13]. The proposed models are conservative in the sense that the local and global values of the phase-field, and therefore mass, is constant throughout the computational domain. Our model is derived using the central moment framework of the cascaded LBM [14, 15]. For simplicity, a single-relaxation-time (SRT) model is formulated. The generalization to multi-relaxation-time (MRT) in the framework of central moments is straightforward but not considered here.

II. GOVERNING EQUATION: CONSERVATIVE PHASE-FILED MODEL

For identification of each of the two phases we use the phase indicator function $\phi(\vec{x}, t)$, where $\vec{x}$ is the position vector and t is the time. The phase indicator is related to the phase flux density $\vec{j}$ by

$$\frac{\partial \phi}{\partial t} = -\nabla \cdot \vec{j}. \tag{1}$$

The flux density is the sum of the advective flux density $\vec{j}_A$, the diffusive flux density $\vec{j}_D$, and the phase separation flux density $\vec{j}_S$:

$$\vec{j} = \vec{j}_A + \vec{j}_D + \vec{j}_S, \tag{2}$$

$$\vec{j}_A = \phi \vec{u}, \tag{3}$$

$$\vec{j}_D = -M \nabla \phi, \tag{4}$$

where $\vec{u}$ is the velocity vector and M is the mobility. The phase separation flux density $\vec{j}_S$ is a function of the phase indicator ϕ that is supposed to impose a predefined interface profile. The interface profile is a smooth approximation of a step function that can move freely on a Cartesian grid. Here we choose a hyperbolic tangent profile

$$\phi^{eq} = \frac{1}{2} \tanh\left(\frac{2(\xi_n - \xi_0)}{W}\right), \tag{5}$$

where ξ_n is the spatial variable normal to the interface located at ξ_0 and the interface width is adjusted by the parameter W. The phase indicator takes on values ± 0.5 in two different phases. In order for $\vec{j}_S$ to impose this profile it has to counteract the diffusive flux $\vec{j}_D$ in such a way that $\vec{j}_D + \vec{j}_S = 0$ for the equilibrium profile given in Eq. (5). Evaluating $\vec{j}_D$ for

the equilibrium profile gives

$$\begin{aligned}\vec{j}_D^{eq} =& - M\nabla\left[\frac{1}{2}\tanh\left(\frac{2(\xi_n-\xi_0)}{W}\right)\right]\\ =& -\frac{M}{2}\vec{n}\frac{\partial}{\partial\xi_n}\tanh\left(\frac{2(\xi_n-\xi_0)}{W}\right)\\ =& -\frac{M}{W}\vec{n}\left[1-\tanh^2\left(\frac{2(\xi_n-\xi_0)}{W}\right)\right],\end{aligned} \tag{6}$$

which can be recast into

$$\vec{j}_D^{eq} = -M\vec{n}\frac{1-4(\phi^{eq})^2}{W}, \tag{7}$$

with the normal vector of the interface defined by:

$$\vec{n} = \frac{\nabla\phi}{|\nabla\phi|}. \tag{8}$$

By specifying $\vec{j}_S$ as

$$\vec{j}_S = M\frac{\nabla\phi}{|\nabla\phi|}\frac{1-4\phi^2}{W} \tag{9}$$

we devise a phase separation flux density that cancels out with the diffusive flux density for the hyperbolic tangent profile. This hyperbolic tangent profile is then the state to which the spatial distribution of ϕ is attracted. Therefore, the following equation should be solved in order to track the interface:

$$\begin{aligned}\frac{\partial\phi}{\partial t} =& -\nabla\cdot\vec{j},\\ \vec{j} =& \phi\vec{u} - M\nabla\phi + M\frac{\nabla\phi}{|\nabla\phi|}\frac{1-4\phi^2}{W},\end{aligned} \tag{10}$$

which can be rewritten as

$$\frac{\partial\phi}{\partial t} + \nabla\cdot(\phi\vec{u}) = \nabla\cdot\left[M\left(\nabla\phi - \frac{\nabla\phi}{|\nabla\phi|}\frac{1-4\phi^2}{W}\right)\right]. \tag{11}$$

This is the target interface-tracking equation in conservative form. Basically, it is the phase-field version of the modified Allen-Cahn equation [10] as proposed by Sun and Beckermann in its general form [11] and later on reformulated by Chiu and Lin in the conservative form [12].

It is worth mentioning that there are some differences between the Cahn-Hilliard and Allen-Cahn equations. The Cahn-Hilliard equation is a 4th-order partial differential equation (PDE) while the Allen-Cahn equation is a 2nd-order PDE that is easier to solve. The phase field in the Cahn-Hilliard theory is conservative and driven by diffusion, while that in the

original Allen-Cahn theory is non-conservative and driven by curvature. Thus, several efforts have been made to improve the simpler Allen-Cahn approach such that the curvature driven dynamics is removed [11] and the governing equation is written in a conservative form [12], which would still be a 2nd-order PDE known as the conservative phase-field equation, Eq. (11). This equation will be solved using a conservative LB model presented in the following section.

III. CONSERVATIVE PHASE-FIELD LATTICE BOLTZMANN METHOD

The interface tracking equation, Eq. (11), is written in the conservative form and a nice property of the LBM is that it retains the conservative properties of the equation being discretized provided that the conserved quantity is implemented as a collision invariant. For the advection-diffusion equation in two dimensions (2D), the minimum number of required microscopic velocities in discretization of the LBE appears to be only five (D2Q5 model) [16]. In order to use the same discretization as in an LB fluid solver we use the nine velocity lattice (D2Q9 model). Needless to say, the discrete D2Q5 model is inferior to the D2Q9 lattice in terms of isotropy and accuracy.

A. The lattice Boltzmann equation

First, we briefly recall some basic properties of LBE. The LBM is a discrete evolution equation for the probability density function f_{ij} that can be written in a general form as:

$$f_{ij}(\vec{x} + \vec{e}_{ij}\Delta t, t + \Delta t) = f_{ij}(\vec{x}, t) + \Omega_{ij}\left(f(\vec{x}, t)\right), \tag{12}$$

where the Miller indices i, j denote the Cartesian lattice directions in 2D and $\vec{e}_{ij} = \{i, j\}$ is the microscopic velocity set chosen such that each part of the distribution f_{ij} moves to a neighboring node on a Cartesian lattice in one time step Δt. This way of discretizing the advection part is called perfect shift. The collision operator Ω_{ij} has to be specified in accordance with the differential equation that is supposed to be solved. It can be shown by asymptotic analysis that the LBE solves a hierarchy of transport equations for the statistical moments of f_{ij}. The SRT is commonly used to simplify the collision operator by specifying

an equilibrium distribution f_{ij}^{eq} and a relaxation parameter ω:

$$\Omega_{ij}^{SRT} = -\omega(f_{ij} - f_{ij}^{eq}), \tag{13}$$

which leads to the popular SRT-LBM.

B. Derivation of the phase-field lattice Boltzmann equation

We devise a local distribution function h_{ij} with the lattice directions indicated by the Miller indices $i, j \in \{\bar{1}, 0, 1\}$ (the over-bar denotes a "minus" in the Miller nomenclature). The discretization uses a native LBM with a local collision operator and the perfect shift solution for the streaming step. It is hence sufficient to discuss the collision rule here. For all lattice quantities we introduce the following notations: a plain quantity such as κ_{ij} denotes either a pre-collision state or a conserved quantity; a quantity with an asterisk as in κ_{ij}^* denotes a post-collision state; and an over-bar symbol signifies the average $\bar{\kappa}_{ij} = (\kappa_{ij}+\kappa_{ij}^*)/2$.

The advective flux density $\vec{j}_A$ is supposed to move the phase field according to a given velocity field $\vec{u} = (u_x, u_y)$. A simple way to impose this flux onto the phase field is transforming the distribution h_{ij} into an equivalent set of central moments which is replaced by the velocity $\vec{u}$. This can be done by using the direct central moment transform

$$\kappa_{\alpha\beta} = \sum_i \sum_j h_{ij}(i - u_x/c)^\alpha (j - u_y/c)^\beta, \tag{14}$$

where α and β run from 0 to 2 to recover the nine central moments and $c = \delta x/\delta t = 1$ is the constant lattice speed and is omitted in what follows. Note that δt and δx are the underlying lattice scales for time and length, respectively.

The phase indicator is identified with the moment $\kappa_{00} = \phi$. According to Taylor series expansion, the LB model with the moment κ_{00} taken as collision invariant solves the following equation [17]:

$$\delta t \partial_t \kappa_{00} = -\delta x(\partial_x \bar{\kappa}_{10} + \partial_y \bar{\kappa}_{01}) + \mathcal{O}(\delta t^3, \delta x^3). \tag{15}$$

It is common and convenient to assume diffusive scaling in dimensionless form where $\delta t \sim \delta x^2 \sim \epsilon^2$ [18]. We therefore expand the moments in terms of ϵ

$$\kappa_{\alpha\beta} = \sum_{n=0}^{\infty} \epsilon^n \kappa_{\alpha\beta}^{(n)}. \tag{16}$$

We can insert Eq. (16) into Eq. (15) and replace δt and δx with ϵ^2 and ϵ, respectively. Since $\epsilon \neq 0$ is an arbitrary parameter, the obtained equation is valid if and only if it holds for all powers of ϵ individually. Therefore, to second order in ϵ, we can extract the following equivalent PDE:

$$\partial_t \kappa_{00}^{(0)} = -\partial_x \bar{\kappa}_{10}^{(1)} - \partial_y \bar{\kappa}_{01}^{(1)}. \tag{17}$$

This scaling fits into the usual LB framework where the advection velocity is also of first order [18].

The Galilean transformation of the central moment transform has already taken care of the advective flux. What remains to be done is designing the equations for $\bar{\kappa}_{10}^{(1)}$ and $\bar{\kappa}_{01}^{(1)}$ in such a way that they comply with the requirements for the diffusive and anti-diffusive flux densities $\vec{j}_D$ and $\vec{j}_S$. Applying the asymptotic expansion to the moment $\kappa_{10}^{(1)}$ gives:

$$\kappa_{10}^{(1)} = \kappa_{10}^{*(1)} - \partial_x \bar{\kappa}_{20}^{(0)} - \partial_y \bar{\kappa}_{11}^{(0)}. \tag{18}$$

We now introduce a collision model for the moment κ_{10} based on the relaxation frequency ω (inverse of the relaxation time τ_h)

$$\kappa_{10}^{*} = \kappa_{10}(1-\omega) + \omega \kappa_{10}^{eq}. \tag{19}$$

The equilibrium moment κ_{10}^{eq} has to be matched to the target equation. Inserting Eq. (19) into Eq. (18) gives:

$$\kappa_{10}^{(1)} = \kappa_{10}^{eq(1)} - \frac{1}{\omega}\left(\partial_x \bar{\kappa}_{20}^{(0)} + \partial_y \bar{\kappa}_{11}^{(0)}\right), \tag{20}$$

$$\kappa_{10}^{*(1)} = \kappa_{10}^{eq(1)} - \left(\frac{1}{\omega} - 1\right)\left(\partial_x \bar{\kappa}_{20}^{(0)} + \partial_y \bar{\kappa}_{11}^{(0)}\right), \tag{21}$$

$$\bar{\kappa}_{10}^{(1)} = \kappa_{10}^{eq(1)} - \left(\frac{1}{\omega} - \frac{1}{2}\right)\left(\partial_x \bar{\kappa}_{20}^{(0)} + \partial_y \bar{\kappa}_{11}^{(0)}\right). \tag{22}$$

A similar result is obtained for $\bar{\kappa}_{01}$ by permuting the indices. Eq. (22) will produce the correct diffusive flux if $\bar{\kappa}_{11}^{(0)} = 0$ and $\bar{\kappa}_{20}^{(0)} \propto \phi$. It can be shown by asymptotic analysis that to the required zeroth order

$$\bar{\kappa}_{\alpha\beta}^{(0)} = \kappa_{\alpha\beta}^{*(0)} = \kappa_{\alpha\beta}^{(0)} = \kappa_{\alpha\beta}^{eq(0)}. \tag{23}$$

It is therefore sufficient to specify appropriate equilibria for the moments κ_{20}, κ_{11}, and κ_{02}.

We have hence determined minimal requirements for the moments to solve the target diffusion problem. The remaining moments κ_{12}, κ_{21}, and κ_{22} are arbitrary according to our

analysis. Numerical methods in general and LBM in particular always leave some freedom beyond the basic requirements of the PDE. For the sake of simplicity we settle with the simplest possible choice and use the SRT. This is done by choosing the same relaxation parameters for all the moments

$$\kappa^*_{00} = \kappa_{00}(1-\omega) + \omega\kappa_{00}, \tag{24}$$

$$\kappa^*_{10} = \kappa_{10}(1-\omega) + \omega\kappa^{eq}_{10}, \tag{25}$$

$$\kappa^*_{01} = \kappa_{01}(1-\omega) + \omega\kappa^{eq}_{01}, \tag{26}$$

$$\kappa^*_{20} = \kappa_{20}(1-\omega) + \omega c_s^2\kappa_{00}, \tag{27}$$

$$\kappa^*_{02} = \kappa_{02}(1-\omega) + \omega c_s^2\kappa_{00}, \tag{28}$$

$$\kappa^*_{11} = \kappa_{11}(1-\omega), \tag{29}$$

$$\kappa^*_{12} = \kappa_{12}(1-\omega) + \omega c_s^2\kappa^{eq}_{10}, \tag{30}$$

$$\kappa^*_{21} = \kappa_{21}(1-\omega) + \omega c_s^2\kappa^{eq}_{01}, \tag{31}$$

$$\kappa^*_{22} = \kappa_{22}(1-\omega) + \omega c_s^4\kappa_{00}. \tag{32}$$

The equilibria for the first order moments κ^{eq}_{10} and κ^{eq}_{01} will be derived shortly. The equilibria for the other moments are determined as follows: The parameter c_s^2 in the moments κ^*_{20} and κ^*_{02} adjusts the variance of the distribution function. The value $c_s^2 = 1/3$ is the solution for the optimization problem that minimizes the defect of Galilean invariance as explained in [15]. Likewise, choosing $\kappa^{eq}_{12} = c_s^2\kappa^{eq}_{10}$ and $\kappa^{eq}_{21} = c_s^2\kappa^{eq}_{01}$ optimizes the isotropy. Since the equilibrium is a joint probability density function for the random particle velocities in the x- and y-directions the equilibrium for the fourth-order moment κ_{22} must be the product of κ^{eq}_{20} and κ^{eq}_{02} normalized by the density [15, 19]. Since we choose to use SRT, we can write the collision operator directly in distribution space thereby avoiding a costly moment transform. The price that we pay is that all the moments are forced to relax with the same rate which might impose limitations on the accuracy and stability of the method. Using this SRT collision with $\kappa^{eq}_{20} = \kappa^{eq}_{02} = c_s^2\kappa_{00} = c_s^2\phi$ and $\kappa^{eq}_{11} = 0$, Eq. (22) becomes

$$\bar{\kappa}^{(1)}_{10} = \kappa^{eq(1)}_{10} - c_s^2\left(\frac{1}{\omega} - \frac{1}{2}\right)\partial_x\phi. \tag{33}$$

We hence identify the mobility as

$$M = \delta t c_s^2\left(\frac{1}{\omega} - \frac{1}{2}\right) = \frac{1}{3}\left(\frac{1}{\omega} - \frac{1}{2}\right). \tag{34}$$

The anti-diffusion flux density $\vec{j}_S$ is implemented in the equilibrium via

$$\kappa_{10}^{eq} = \left(\frac{\nabla\phi}{|\nabla\phi|}\right)_x \left(\frac{1}{\omega} - \frac{1}{2}\right) \frac{1-4\phi^2}{3W} = \frac{1}{|\nabla\phi|} \left(\frac{1}{\omega} - \frac{1}{2}\right) \frac{1-4\phi^2}{3W} \partial_x\phi, \tag{35}$$

$$\kappa_{01}^{eq} = \left(\frac{\nabla\phi}{|\nabla\phi|}\right)_y \left(\frac{1}{\omega} - \frac{1}{2}\right) \frac{1-4\phi^2}{3W} = \frac{1}{|\nabla\phi|} \left(\frac{1}{\omega} - \frac{1}{2}\right) \frac{1-4\phi^2}{3W} \partial_y\phi. \tag{36}$$

Eqs. (35) and (36) are designed to lead to the target equation, Eq. (11), for the flux density $\vec{j}$ when inserted into Eq. (17) via Eq. (33). The only difficulty in doing this appears to be the determination of the interface normal. However if we insert Eq. (35) into Eq. (20) and do the same for the moment κ_{01} we obtain

$$\kappa_{10}^{(1)} = \frac{1}{|\nabla\phi|} \left(\frac{1}{\omega} - \frac{1}{2}\right) \frac{1-4\phi^2}{3W} \partial_x\phi - \frac{1}{3} \left(\frac{1}{\omega} - \frac{1}{2}\right) \partial_x\phi = \Lambda \partial_x\phi, \tag{37}$$

$$\kappa_{01}^{(1)} = \frac{1}{|\nabla\phi|} \left(\frac{1}{\omega} - \frac{1}{2}\right) \frac{1-4\phi^2}{3W} \partial_y\phi - \frac{1}{3} \left(\frac{1}{\omega} - \frac{1}{2}\right) \partial_y\phi = \Lambda \partial_y\phi. \tag{38}$$

While the prefactor Λ is *a priori* unknown, it is the same for both κ_{10} and κ_{01}. The normal can hence be easily computed from the pre-collision central moments by

$$n_x = \left(\frac{\nabla\phi}{|\nabla\phi|}\right)_x = -\frac{\kappa_{10}}{\sqrt{\kappa_{10}^2 + \kappa_{01}^2}}, \tag{39}$$

$$n_y = \left(\frac{\nabla\phi}{|\nabla\phi|}\right)_y = -\frac{\kappa_{01}}{\sqrt{\kappa_{10}^2 + \kappa_{01}^2}}. \tag{40}$$

The collision for the central moments κ_{10} and κ_{01} can be summarized as

$$\kappa_{10}^* = \kappa_{10}(1-\omega) - \frac{\kappa_{10}}{\sqrt{\kappa_{10}^2 + \kappa_{01}^2}} \frac{1-4\phi^2}{6W} (2-\omega), \tag{41}$$

$$\kappa_{01}^* = \kappa_{01}(1-\omega) - \frac{\kappa_{01}}{\sqrt{\kappa_{10}^2 + \kappa_{01}^2}} \frac{1-4\phi^2}{6W} (2-\omega). \tag{42}$$

With the equilibrium at hand, it is also possible to compute the gradient of ϕ directly by inserting the equilibrium moments into Eq. (20):

$$\partial_x\phi = -3\omega \left(\kappa_{10} - \frac{\kappa_{10}}{\sqrt{\kappa_{10}^2 + \kappa_{01}^2}} \frac{1-4\phi^2}{3W} \left(\frac{1}{\omega} - \frac{1}{2}\right)\right) + \mathcal{O}(\epsilon^2), \tag{43}$$

$$\partial_y\phi = -3\omega \left(\kappa_{01} - \frac{\kappa_{01}}{\sqrt{\kappa_{10}^2 + \kappa_{01}^2}} \frac{1-4\phi^2}{3W} \left(\frac{1}{\omega} - \frac{1}{2}\right)\right) + \mathcal{O}(\epsilon^2). \tag{44}$$

The asymptotic analysis in this section does not account for grid-scale oscillations which are commonly observed in LB simulations. Grid scale oscillations in the gradient computation can produce artifacts at the interface. Since they are not predicted by asymptotic analysis we need to investigate them numerically.

C. Single-relaxation-time LBM

Since, for the sake of simplicity, we decided to use the SRT-LBM we can write the LBE directly in distribution form:

$$h_{ij}(\vec{x}+\vec{e}_{ij}\Delta t, t+\Delta t) = h_{ij}(\vec{x},t) - \omega(h_{ij}(\vec{x},t) - h_{ij}^{eq}(\vec{x},t)). \tag{45}$$

In order to recover the conservative phase-field equation, Eq. (11), we obtain the following equilibrium distribution by transforming the equilibrium central moments of Eqs. (24)–(32) into distribution space and dropping terms of third and fourth order in velocity

$$h_{ij}^{eq} = \phi w_{ij}\left[1 + \frac{\vec{e}_{ij}\cdot\vec{u}}{c_s^2} + \frac{(\vec{e}_{ij}\cdot\vec{u})^2}{2c_s^4} - \frac{\vec{u}\cdot\vec{u}}{2c_s^2}\right] + Bw_{ij}\left(\vec{e}_{ij}\cdot\vec{n}\right). \tag{46}$$

We adopted the standard SRT nomenclature with the weight coefficients w_{ij} that can be calculated from:

$$w_{ij} = \frac{4^{1-|i|-|j|}}{9}. \tag{47}$$

The anti-diffusion part of equilibrium has been absorbed into the coefficient B

$$B = \frac{M}{c_s^2}\frac{(1-4\phi^2)}{W}, \tag{48}$$

in which the mobility is given by Eq. (34).

The interface normal can be computed either by using isotropic finite differences or by Eqs. (39) and (40).

Notice that in this approach we chose the relaxation frequency as the only means to adjust the mobility such that c_s^2 remains at its optimum [15]. This is in contrast to other studies that control the mobility independent of the relaxation time. For example, the mobility in Ref. [4] is $M = \Gamma\left(\tau_h - 0.5\right)\delta t$ while in Refs. [2, 5] it is defined as $M = \eta c_s^2\left(\tau_h - 0.5\right)\delta t$, where Γ and η are additional free parameters for tunning the mobility.

IV. NUMERICAL VALIDATION

Four different benchmark problems including diagonal motion of a circular interface, Zalesak's rotating disk [20], circular interface in a shear flow [21] and in a deformation field [22] are considered to assess the accuracy of the proposed conservative LBE model. Unless otherwise is specified, the following parameters, quantified in lattice units, are used in the

simulations: $M = 0.001$, $U_0 = 0.02$, and $W = 3$. In other words, the Péclet number of the flow

$$\mathrm{Pe} = \frac{U_0 W}{M} \tag{49}$$

is kept constant at $\mathrm{Pe} = 60$. The results are compared with the previous studies by Zu and He [4] and the SRT version of the MRT model proposed by Liang *et al.* [5]. Because both aforementioned models produce very similar results only one of them will be shown. Of note is that the definition of the Péclet number in Refs. [4, 5] is slightly different due to presence of the chemical potential. In our simulations we made sure that both Péclet numbers match.

The relative error between the numerical results and the analytical solution is calculated using the following formula:

$$\|\delta\phi\|_2 = \sqrt{\frac{\sum\limits_{x,y} \left(\phi - \phi_0\right)^2}{\sum\limits_{x,y} \phi_0^2}}, \tag{50}$$

where ϕ_0 is the initial value of the phase field at $T = 0$. The time scale is defined by

$$T_f = \frac{L_0}{U_0}, \tag{51}$$

where L_0 is size of the domain.

A. Diagonal translation of a circular interface

First we consider the motion of a circular interface due to a constant velocity field $\vec{u} = (U_0, U_0)$. This is similar to the hydrodynamic Galilean invariance test for multiphase flows. Initially, a circular interface with radius $R = L_0/4$ is placed in the middle of a periodic domain with $L_0 \times L_0$ lattice cells with $L_0 = 100$. The initial profile of the interface and the final shape after 10 cycles are plotted in Fig. 1.

As can be seen in Fig. 1(a), there is a noticeable shift between the initial and final shapes of the interface when the SRT methods presented in Refs. [4, 5] are used. On the other hand, the proposed conservative LB models produce more accurate results. Particularly, when finite differences are used to calculate the normal to the interface in Fig. 1(b) the final shape of the bubble coincides very well with its initial configuration. The computation of the interface normal using central moments obviously has some disadvantages with regard to accuracy when compared to the model that uses FD. The deformations of the interface seen

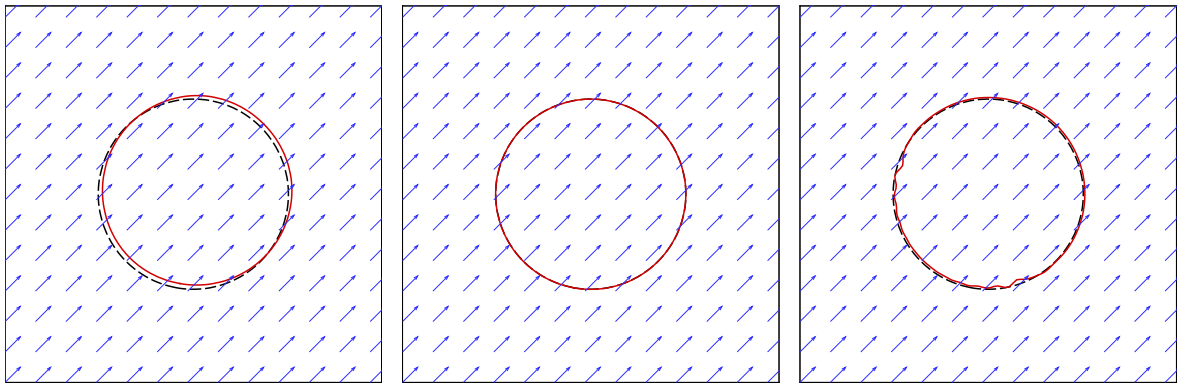

(a) (b) (c)

FIG. 1. (Color online) Diagonal translation of a circular interface at Pe = 60. The phase-field contour ($\phi = 0$) is shown: Black dashed lines represent the initial profile ($T = 0$) and red solid lines show the interface after 10 cycles ($T = 10T_f$). (a) Results of the proposed SRT model of Refs. [4, 5] and conservative LBM using (b) finite differences and (c) moments to compute the interface normal.

in Fig. 1(c) indicate that some grid scale oscillations exist in the computation of the normal to the interface using central moments. This is certainly a disadvantage of the moment approach. However, it is important to note that the moment-based model used in Fig. 1(c) is completely local. The relative error of the simulations based on Eq. (50) is provided in Table I.

TABLE I. Relative error based on Eq. (50) for different models and different case studies.

case study	diagonal motion	Zalesak's disk	shear flow	deformation	smooth deformation
SRT model of Refs. [4, 5]	0.1176	0.1401	0.0403	0.0551	0.0311
Current (FD)	0.0074	0.1404	0.0216	0.0570	0.0333
Current (moment)	0.0874	0.1406	0.0274	0.0622	0.0380

B. Zalesak's rotation of a slotted disk

Zalesak's disk rotation [20] is another benchmark study used for validation of the interface tracking equations. The initial condition is a slotted disk with radius $R = 80$ in the middle of a periodic domain with $L_0 \times L_0$ lattice sites where $L_0 = 200$. The width of the slot is 15 lattice cells centered in the middle of the domain as shown in Fig. 2. The velocity field is given by

$$\begin{cases} u_x(x,y) = & -U_0\pi\left(\dfrac{y}{L_0} - 0.5\right) \\ u_y(x,y) = & U_0\pi\left(\dfrac{x}{L_0} - 0.5\right). \end{cases} \tag{52}$$

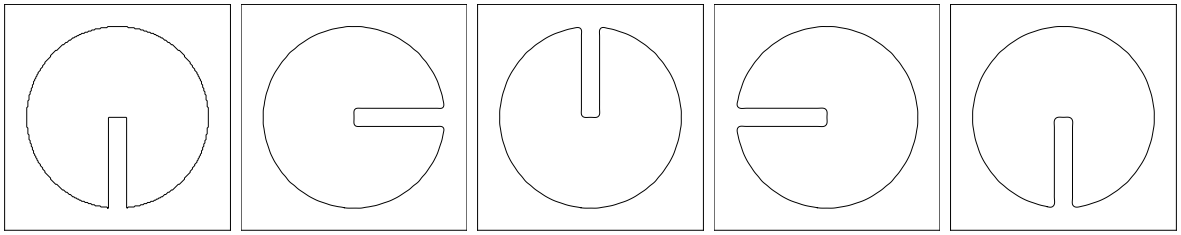

(a)$T = 0$ (b)$T = T_f/2$ (c)$T = T_f$ (d)$T = 3T_f/2$ (e)$T = 2T_f$

FIG. 2. Rotation of the Zalesak's disk with time.

The initial shape of the disk together with its final shape at $T = 2T_f$ is shown in Fig. 3. As it can be observed, there is a slight discrepancy between the initial and final position of the slotted disk. The relative errors in the calculations provided in Table I are almost identical for all the methods examined here. Both FD-based and moment-based computation of the interface normal reproduce satisfactory results as can be seen in Fig. 3(b) and Fig. 3(c).

C. Circular interface in a shear flow

Next, we place a circular interface in a periodic domain subject to the following shear flow [21]:

$$\begin{cases} u_x(x,y) = & -U_0\pi\cos\left[\pi\left(\dfrac{x}{L_0} - 0.5\right)\right]\sin\left[\pi\left(\dfrac{y}{L_0} - 0.5\right)\right], \\ u_y(x,y) = & U_0\pi\sin\left[\pi\left(\dfrac{x}{L_0} - 0.5\right)\right]\cos\left[\pi\left(\dfrac{y}{L_0} - 0.5\right)\right]. \end{cases} \tag{53}$$

The initial radius of the circular interface is $R = L_0/5$ and it is placed at $(x, y) = (100, 60)$ in a computational domain with $L_0 \times L_0$ lattice cells where $L_0 = 200$. In order for the

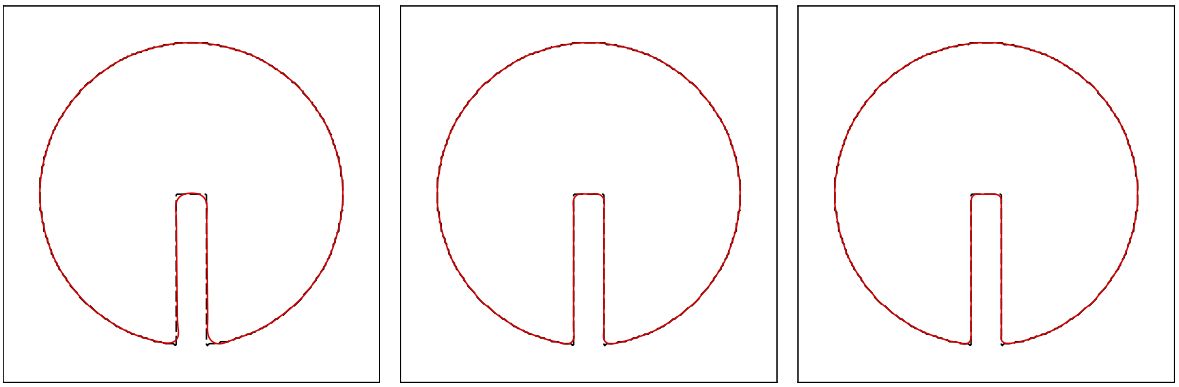

(a) (b) (c)

FIG. 3. (Color online) Zalesak's disk at Pe = 60. The phase-field contour ($\phi = 0$) is shown at $T = 0$ (black dashed line) and $T = 2T_f$ (red solid line). (a) Results of the SRT model of Refs. [4, 5] and conservative LBM using (b) finite differences and (c) moments to compute the interface normal.

interface to get back to its original position the velocity field is reversed at $T = T_f$ and the simulation is carried on until $T = 2T_f$. The evolution of the interface at different times is demonstrated in Fig. 4.

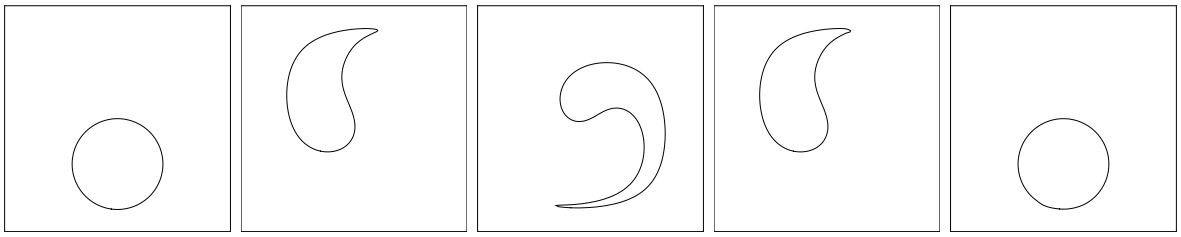

(a)$T = 0$ (b)$T = T_f/2$ (c)$T = T_f$ (d)$T = 3T_f/2$ (e)$T = 2T_f$

FIG. 4. Evolution of a circular interface under shear flow.

The shapes of the interface at $T = T_f$ and $T = 2T_f$ are shown in Fig. 5. As it can be seen, the results are in good agreement with the theoretical predictions.

D. Deformation of a circular interface

The last benchmark study considered is deformation of a circular interface due to the following velocity field [5, 22]:

$$\begin{cases} u_x(x,y) = -U_0 \sin\left[4\pi\left(\frac{x}{L_0}+0.5\right)\right] \sin\left[4\pi\left(\frac{y}{L_0}+0.5\right)\right], \\ u_y(x,y) = -U_0 \cos\left[4\pi\left(\frac{x}{L_0}+0.5\right)\right] \cos\left[4\pi\left(\frac{y}{L_0}+0.5\right)\right]. \end{cases} \tag{54}$$

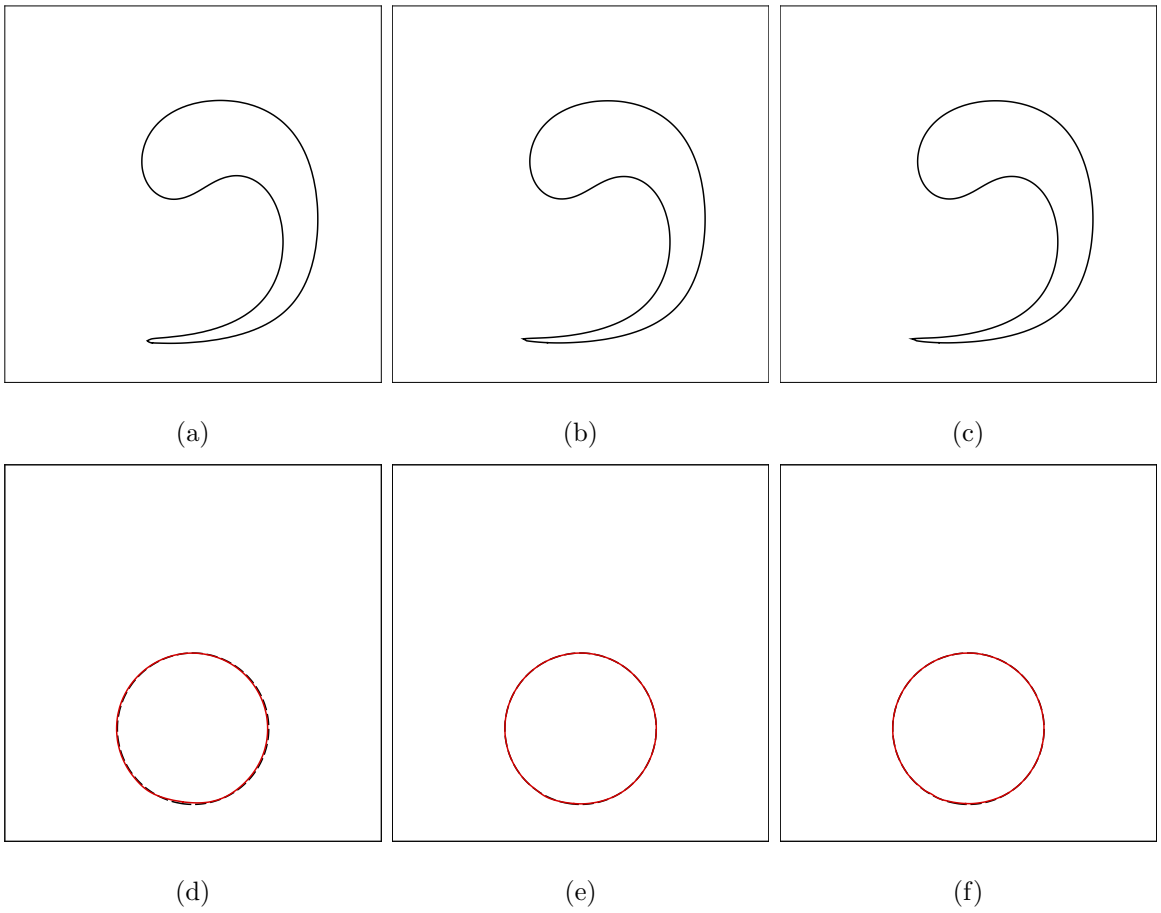

FIG. 5. A circular interface under shear flow at Pe = 60. The phase-field contour ($\phi = 0$) is shown at $T = T_f$ (upper row) and $T = 2T_f$ (lower row). (a),(d) Results of the SRT model of Refs. [4, 5]; (b),(e) conservative LBM using finite differences; (c),(f) conservative LBM using moments to compute the interface normal.

The initial condition is a circular interface with $R = L_0/5$ in the middle of a periodic domain with $L_0 \times L_0$ lattice cells where $L_0 = 500$. The velocity field is reversed at $T = T_f/2$ so that the interface goes back to its original position, and the simulation continues until $T = T_f$. The topological changes of the interface at different times is depicted in Fig. 6.

The shape of the interface at $T = T_f/2$ and $T = T_f$ is shown in Fig. 7. As pointed out by Liang *et al.* [5], and as can be observed from our findings, this is a very rigorous benchmark case because the interface undergoes a severe topological change. The wiggles appearing at $T = T_f$ in Fig. 7(d)–7(f) are mainly due to the disintegration and reconsolidation of the interface, which are due to the stringent initial velocity field and rapid shift in its direction at $T = T_f/2$. In order to affirm this speculation, a smoothed version of the velocity field, as

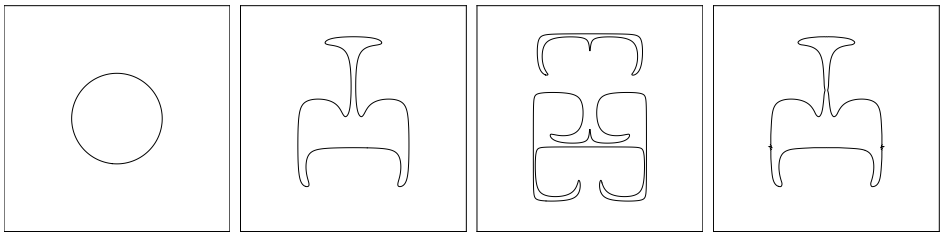

(a)$T = 0$ (b)$T = T_f/4$ (c)$T = T_f/2$ (d)$T = 3T_f/4$

FIG. 6. Evolution of a circular interface subject to a deformation flow field.

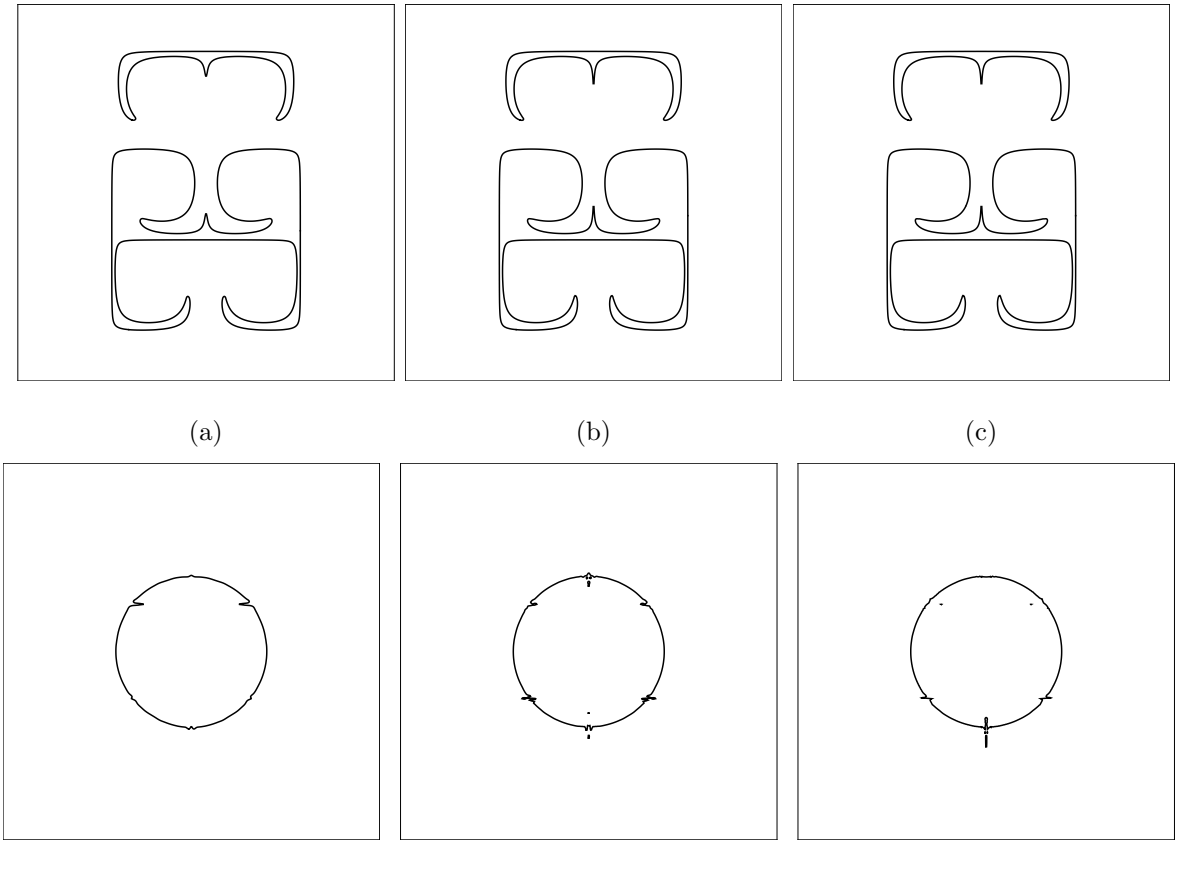

(a) (b) (c)

(d) (e) (f)

FIG. 7. Deformation of a circular interface at Pe = 60. The phase-field contour ($\phi = 0$) is shown at $T = T_f/2$ (upper row) and $T = T_f$ (lower row). (a),(d) Results of the SRT model of Refs. [4, 5]; (b),(e) conservative LBM using finite differences; (c),(f) conservative LBM using moments to compute the interface normal.

used in Ref. [5], is implemented. In other words, instead of imposing a sharp velocity field and suddenly reversing its direction, we multiply the velocity field in Eq. (54) by $\cos(\frac{\pi T}{T_f})$.

The deformation of the interface due to a smooth velocity field is shown in Fig. 8. Com-

paring Fig. 7 and Fig. 8 at $T = T_f/2$, we observe that the interface subjected to the smoothed velocity field is not disintegrated and is less deformed. Accordingly, a lesser numerical error is induced when the convoluted interface stretches back to its original configuration. The relative error of the simulations given in Table I further confirms our explanation.

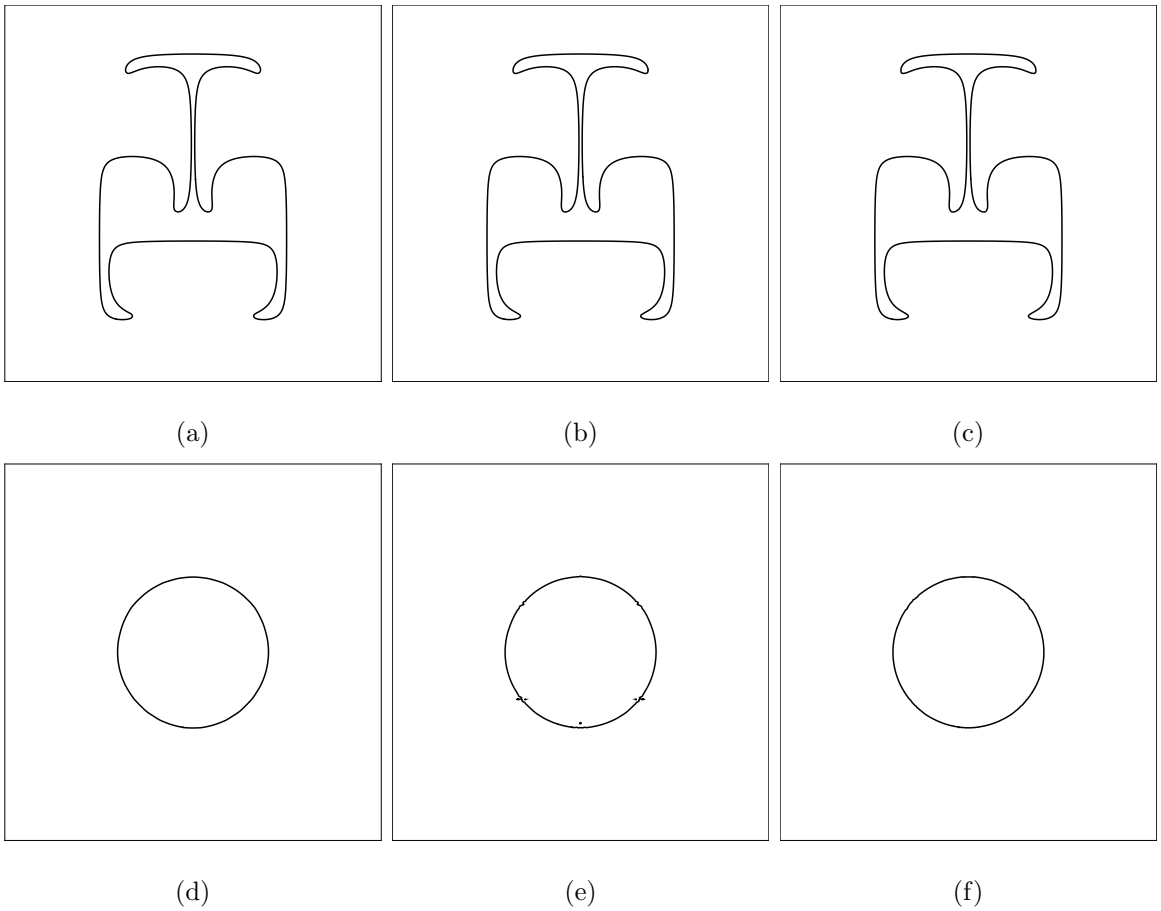

FIG. 8. Deformation of a circular interface at Pe = 60 subjected to a smoothed velocity field. The phase-field contour ($\phi = 0$) is shown at $T = T_f/2$ (upper row) and $T = T_f$ (lower row). (a),(d) Results of the SRT model of Refs. [4, 5]; (b),(e) conservative LBM using finite differences; (c),(f) conservative LBM using moments to compute the interface normal.

E. Convergence study

Before concluding the paper, we consider the diagonal translation of a circular interface to examine the convergence rate of the presented phase-field LBM at a constant Cahn number $\mathrm{Cn} = \frac{W}{L_0}$. We also compare the current results with those based on the model proposed in

Ref. [4] and the SRT version of the LBM proposed in Ref. [5]. Here, the diffusive scaling is used and the error is measured by calculating the L_2 norm defined in Eq. (50) at $T = T_f$.

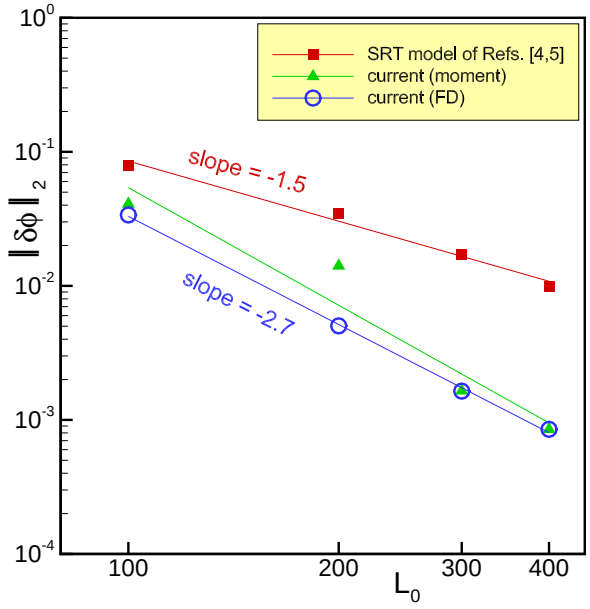

FIG. 9. (Color online) Convergence study: L_2 norm versus number of grid points for the diagonal translation of a circular interface at Pe = 60 and Cn = 0.015.

Keeping the Cahn number constant implies increasing the interface width as we refine the mesh. Because the number of points that resolve the interface increases with W, the numerical error is expected to decrease as the interfacial thickness is increased. This is shown in Fig. 9. As it can be seen, not only the order of accuracy of the current model is higher than that of Refs. [4, 5], the magnitude of the L_2 norm error is also smaller. Of note is that, the moment-based model exhibits an irregular error at $L_0 = 200$ in Fig. 9. It seems that the moment-based approach requires a minimum number of grid points for resolving the interfacial region in order to produce accurate results. Given that $\mathrm{Cn} = W/L_0 = 0.015$, the interface thickness for $L_0 = 200$ is $W = 3$. Apparently, when $W > 4$ the moment-based results become identical to the FD-based results. This speculation is currently under investigation and will be addressed in our future study.

V. SUMMARY

An LB model for tracking the interface between different phases was proposed in this study. The governing conservative phase-field equation requires only 1st-order derivative, or

even no derivatives if moments are utilized in the calculation of the interface normal. The numerical studies suggest that when finite difference is used to compute the gradient of the phase field the solution could be slightly more accurate but the price we pay is a non-local collision operator. The main reason for the lack of accuracy in the moment method seems to be linked to grid-scale oscillations in the computation of the gradients. The FD method does not seem to be susceptible to this problem though. In the considered test cases the grid scale oscillations did not blow up the numerical results but they are certainly unwanted. Their complete elimination is the subject of our future investigations.

On the other hand, the focus of the present study was to propose a phase-field LBM for interface tracking with an entirely local collision operator thereby achieving higher efficiency on parallel machines. As such, we confined the proposed LBM to the single-relaxation-time model. Consequently, the Péclet number of the flow was limited to relatively low values (Pe ~ 100) in order to obtain numerically stable results. Extension of the current SRT-LBM to multi-relaxation-time [5] or models based on the concept of cumulants also constitutes the subject of our future work.

Using moments in the computation of gradients makes the update process completely local and allows for the application of all optimization techniques which are available to accelerate, parallelize, and reduce the memory foot-print of the native lattice Boltzmann method [23] (AA-Pattern [24], EsoTwist [25], etc.). The computation of finite differences is usually incompatible with these optimization techniques. The application of a hybrid LB/FD method slows down the computation in two ways: First, the non-local finite differences require additional read and write operations. Second, the usual optimization for native LB codes cannot be applied and one has to settle with data structures and algorithms which are not optimal for the LBM. In the current study we deliberately used non-optimized code such that we could directly compare the accuracy of the hybrid methods with the all-native lattice Boltzmann method. The error produced by our conservative phase-field model is less than the error resulted from other existing LB models for the range of parameters studied.

ACKNOWLEDGMENTS

MG thanks the German Research Foundation (DFG) Research Training Group FOR 1083 (MUSIS) Project P2 "Pore scale simulation of energy and mass flux in 3D unsaturated

porous media" grand number KR 1747/13-2 for financial support. AF and TL acknowledge the funding from the DOE's NEUP.

REFERENCES

[1] X. He and L.-S. Luo, Phys. Rev. E **56**, 6811 (1997).

[2] A. Fakhari and M. H. Rahimian, Phy. Rev. E **81**, 036707 (2010).

[3] T. Lee and L. Liu, J. Comput. Phys. **229**, 8045 (2010).

[4] Y. Q. Zu and S. He, Phy. Rev. E **87**, 043301 (2013).

[5] H. Liang, B. C. Shi, Z. L. Guo, and Z. H. Chai, Phy. Rev. E **89**, 053320 (2014).

[6] A. Fakhari and T. Lee, Phys. Rev. E **87**, 023304 (2013).

[7] T. J. Spencer, I. Halliday, and C. M. Care, Phil. Trans. R. Soc. A **369**, 2255 (2011).

[8] J. Tölke, G. D. Prisco, and Y. Mu, Comput. Math. Appl. **65**, 864 (2013).

[9] J. W. Cahn and J. E. Hilliard, J. Chem. Phys. **28**, 258 (1958).

[10] S. M. Allen and J. W. Cahn, Acta Metall. **24**, 425 (1976).

[11] Y. Sun and C. Beckermann, J. Comput. Phys. **220**, 626 (2007).

[12] P.-H. Chiu and Y.-T. Lin, J. Comput. Phys. **230**, 185 (2011).

[13] T. Lee and C.-L. Lin, J. Comput. Phys. **206**, 16 (2005).

[14] M. Geier, A. Greiner, and J. G. Korvink, Phys. Rev. E **73**, 066705 (2006).

[15] M. Geier, *Ab initio derivation of the cascaded lattice Boltzmann automaton*, Ph.D. thesis, Albert-Ludwigs University Freiburg (2006).

[16] H. W. Zheng, C. Shu, and Y. T. Chew, Phy. Rev. E **72**, 056705 (2005).

[17] F. Dubois, Comput. Math. Appl. **55**, 1441 (2008).

[18] M. Junk, A. Klar, and L.-S. Luo, J. Comput. Phys. **210**, 676 (2005).

[19] M. Geier, A. Greiner, and J. G. Korvink, Eur. Phys. J. Special Topics **171**, 55 (2009).

[20] S. T. Zalesak, J. Comput. Phys. **31**, 335 (1979).

[21] M. Rudman, Int. J. Num. Meth. Fluids **24**, 671 (1997).

[22] W. J. Rider and D. B. Kothe, J. Comput. Phys. **141**, 112 (1998).

[23] M. Wittmann, T. Zeiser, G. Hager, and G. Wellein, Comput. Math. Appl. **65**, 924 (2013).

[24] P. Bailey, J. Myre, S. D. C. Walsh, D. J. Lilja, and M. O. Saar, in *Parallel Processing, 2009. ICPP '09. International Conference on* (2009) pp. 550–557.

[25] J. Linxweiler, *Ein integrierter Softwareansatz zur interaktiven Exploration und Steuerung von Strömungssimulationen auf Many-Core-Architekturen*, Ph.D. thesis, TU-Braunschweig (2011).